







Open Archive TOULOUSE Archive Ouverte (OATAO)

OATAO is an open access repository that collects the work of some Toulouse researchers and makes it freely available over the web where possible.

This is an author's version published in : <http://oatao.univ-toulouse.fr/9739>

Official URL : <https://doi.org/10.1016/j.jfluidstructs.2012.11.005>

To cite this version :

Deri, Enrico  and Braza, Marianna  and Cid, Emmanuel  and Cazin, Sébastien  and Michaelis, Dirk and Degouet, Cédric *Investigation of the three-dimensional turbulent near-wake structure past a flat plate by tomographic PIV at high Reynolds number.* (2014) *Journal of Fluids and Structures*, vol. 47. pp. 21-30. ISSN 0889-9746

Any correspondence concerning this service should be sent to the repository administrator : tech-oatao@listes-diff.inp-toulouse.fr

Investigation of the three-dimensional turbulent near-wake structure past a flat plate by tomographic PIV at high Reynolds number

E. Deri^{a,b,*}, M. Braza^a, E. Cid^a, S. Cazin^a, D. Michaelis^c, C. Degouet^d

^a Institut de Mécanique des Fluides de Toulouse (IMFT), UMR 5502 CNRS-INPT-UPS, allée du Prof. Camille Soula, F-31400 Toulouse, France

^b Fondation STAE, 23 av Belin, F-31400 Toulouse, France

^c LaVision GmbH, Anna-Vandenhoeck-Ring 19, D-37081 Göttingen, Germany

^d LaVision France, 5 av de Scandinavie, F-91953 Courtaboeuf, France

ARTICLE INFO

Keywords:

Wake
Flat plate
Tomographic PIV

ABSTRACT

This paper reports an experimental investigation of the high-Reynolds number turbulent flow past a thin flat plate with sharp untapered edges, by means of tomographic PIV. The experiments, carried out in the S4 wind tunnel of IMFT, have quantified the three-dimensional coherent vortex structures, by means of 3-D Proper Orthogonal Decomposition and reconstruction. The interaction of the most energetic coherent structures with the random turbulence is discussed. Furthermore, Proper Orthogonal Decomposition (POD), analysis allowed evaluation of three-dimensional phase-averaged dynamics that quantified the vortex shedding mechanism as well as the influence of higher modes associated with the finer-scale turbulence.

1. Introduction

The present flow is a generic configuration concerning trailing edge unsteady dynamics and flows arising past flaps of micro and nano-drones among other applications. With the rise of developments in aeroacoustics and in micro- and nano-air vehicles design, flat plate aerodynamics gained interest in the last decade (Beckwith and Babinsky, 2009; Hsu and Huang, 2008; Pelletier and Mueller, 2000). In this context, the French foundation *Sciences et Technologies pour l'Aéronautique et l'Espace* launched the EMMAV research program (Electroactive Morphing for Micro Air Vehicles) for the period 2009–2011, as well as the platform SMARTWING in the period 2012–2015. This programme aims at optimising micro-air-vehicles performances in realistic environment by means of electroactive morphing concepts. The present paper concerns a first set of experiments dealing with the static configuration of a flat plate at incidence. Although it is a quite elementary configuration, a rather reduced literature exists on the flow around a thin flat plate with sharp edges. The results of the freefall tests done by Gustave Eiffel from his famous tower in 1911 are available in Rebuffet (1950). Measuring the falling time, the French engineer deduced the normal force coefficient for various aspect ratios. The ninety degrees range of angles of attack is covered with only nine points.

* Corresponding author. Present address: EDF R&D – Fluid Mechanics, Power Generation and Environment Department (MFEE) – 6, quai Watier, F-78401 Chatou, France.

E-mail addresses: enrico.deri@edf.fr (E. Deri), marianna.braza@imft.fr (M. Braza).

Some years later [Fage and Johansen \(1927\)](#) provided more detailed observation of a large span plate with tapered edges for a Reynolds number of 150 000. By means of static pressure measurements over the chord of the plate, the authors evaluated the normal force coefficient at thirteen different angles of attack spanning the range from 0° to 90° . In addition, they performed hot wire anemometry measurements in the wake. The data on the normal force coefficient have been used later by [Wick \(1954\)](#) to investigate the validity of thin airfoil theory. Thirty-five years later, [Abernathy \(1962\)](#) performed some additional Strouhal and pressure measurements on the inclined flat plate: various angles of attack were explored for Reynolds numbers up to 100 000 discussing the influence of span to chord ratio.

Velocity measurements have been performed on the wake behind plates at high incidence including phase averaged fields. Hot Wire Anemometry experiments have been carried out by [Perry and Steiner \(1987\)](#) and [Steiner and Perry \(1987\)](#) for Reynolds numbers up to 37 000 and an angle of attack of 90° . [Leder \(1991\)](#) and [Lam \(1996\)](#) used Laser Doppler Anemometry both for a Reynolds number of about 30 000 for incidences of 30° and 90° . [Lam and Leung \(2005\)](#) performed Particle Image Velocimetry (PIV) at a Reynolds number of 5300 for incidences between 20° and 30° . Finally, [Shi et al. \(2010\)](#) proposed a parametric PIV investigation on bluff plates with chord-to-thickness ratios of 3–9.

A number of numerical studies appeared in the open literature in the last decade for low and high Reynolds number cases ([Breuer et al., 2003](#); [Lam and Wei, 2010](#); [Lee and Lee, 2012](#); [Ouvrard et al., 2010](#)).

Even though several studies on flat plates wakes exist in the open literature, none of them proposes three-dimensional velocity data that can be used further on for high Reynolds number Computational Fluid Dynamic (CFD) improvement and validation. Therefore, the present study and its data-base aims at providing a detailed 3-D data-base by means of tomographic PIV and a physical analysis of a strongly detached unsteady flow useful for the CFD community, beyond the experimental goals of the EMMAV research program.

This paper aims at discussing the behaviour of three dimensional averaged and coherent velocity and vorticity fields in the near wake of a rigid plate at a high Reynolds number ($Re=200\,000$) at incidence of 10° . In [Section 2](#), this paper presents the experimental set-up of the Tomo-PIV carried out in wind tunnel environment. In [Section 3.1](#), Reynolds averaged quantities are discussed including the turbulent stresses fields. In [Section 3.2](#), a Proper Orthogonal Decomposition and reconstruction of the 3-D flow fields is presented. In [Section 3.3](#), phase-averaged dynamics are discussed. [Section 4](#) presents the conclusions.

2. Experimental set-up

The experiments have been carried out in the closed loop wind tunnel S4 of the Institut de Mécanique des Fluides de Toulouse (IMFT) having a turbulence rate of less than 1% ([Chassaing et al., 1974](#)). The test section is 2 m long, 0.7 m tall and 0.6 m large.

The plate is mounted on the walls, spanning the width of the test section, without end plates. The ratio between the chord and the thickness is 20. The ratio between the span and the chord (aspect ratio) is 2. The angle of attack is 10° , resulting in an effective blockage ratio of 0.074 (ratio of the vertical projected surface over the wind tunnel's cross-section). The Reynolds number based on the undisturbed incident velocity, the plate chord and the air viscosity is 200 000 for all the tests. A schematic presentation of the experiment is presented in [Fig. 1](#) together with a view of a larger part of the flow field, by means of CFD simulations carried out within the same research group ([Ouvrard et al., 2010](#)).

Tomographic PIV measurements have been performed using a Flowmaster system from LaVision. The illumination was provided by a double pulsed Nd:YAG laser Quantel, introduced by a mirror from the bottom of the wind tunnel and shaped into a laser sheet of 10 mm thick using LaVision Volume Optics. The laser delivers an energy of 2×200 mJ at 532 nm. A mask slit was added in the path of the laser light to create a sharply defined illuminated domain. A second mirror was fixed at the top side of the closed-loop wind tunnel, reflecting the laser light back toward the measurement volume. This optical double-pass configuration slightly increased the illumination energy ([Gahemi and Scarano, 2010](#)). Three LaVision Imager PRO X cameras (2048×2048 pixels) and a PCO 2000 camera (2048×2048 pixels) are placed along one side of the wind tunnel. The cameras, equipped with Scheimpflug adaptors and 55 mm objective lenses at a diaphragm aperture of 11, observe the illuminated volume of 40 cm^3 with a solid angle of $19^\circ \times 19^\circ$. The system, both cameras and laser, was operated at a frequency of 4 Hz. [Fig. 2](#) shows a picture of the wind tunnel's test-section with the obstacle and the four cameras disposal, as well as an example of instantaneous velocity field by means of Tomo-PIV.

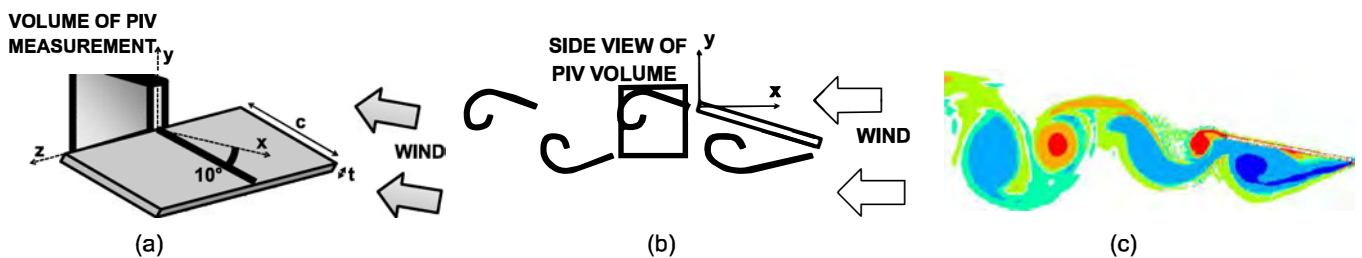


Fig. 1. (a) Schematic representation of the experimental arrangement: the frame origin is on the trailing edge at the middle of the plate's span. (b) Sketch of the flow structure: the side of the measuring volume is about 0.4 chordes. (c) View of phase-averaged iso-vorticity field, CFD simulations by [Ouvrard et al. \(2010\)](#).

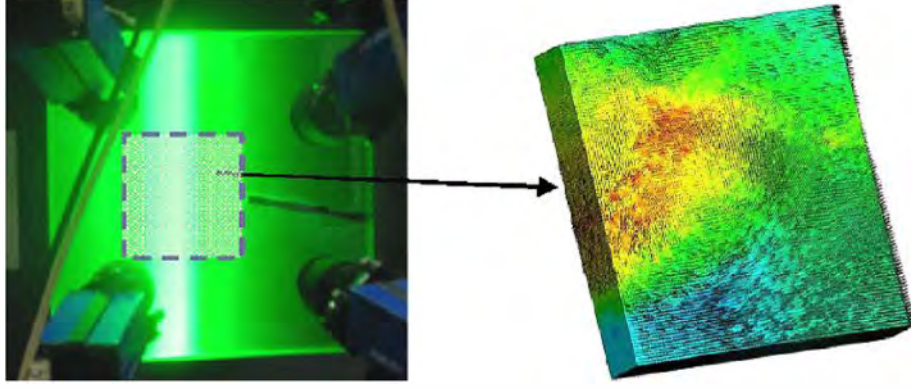


Fig. 2. View of the experimental set-up and of an instantaneous 3-D velocity field.

Six iterations of the Multiplicative Algebraic Reconstruction Technique (MART) are used to reconstruct the tomograms. For each pixel p in each camera and then for each voxel v , the MART algorithm corrects the previous guess E^n by means of the ratio of the measured intensity I to the current intensity

$$E_v^{n+1} = E_v^n \left(\frac{I_p}{\sum_v W_{pv} E_v^n} \right)^{\mu W_{pv}}, \quad (1)$$

where μ is a relaxation parameter and the coefficient w_{pv} weights the contribution E_v of each voxel to the pixel intensity I_p (Elsinga et al., 2006).

Once the volume reconstructed, 40 voxels side cubic interrogation windows are used for three dimensional correlation. The final velocity fields have a size of $0.4 \times 0.4 \times 0.06$ chords and contain 1.3 M vectors each, with a grid spacing of 0.002 chords. A very light removal of “outliers” has been performed by using the method proposed by Westerweel and Scarano (2005) with a threshold of 4 in a $3 \times 3 \times 3$ neighbourhood. A number of 225 three-dimensional flow fields have been reconstructed and correlated. This corresponds to a total data size of 1.3 Tb. Due to post-processing limitations, it was difficult to compare the data with statistics provided by a higher number of snapshots.

3. Results and discussion

In the present section, the instantaneous 3-D flow structure is analysed by means of Reynolds averaging, POD decomposition and phase-averaging, driven by the first two POD modes.

All quantities are made non-dimensional by means of the upstream undisturbed velocity U_∞ and the plate chord c . In the context of statistical (Reynolds) averaging the nomenclature for a generic physical quantity is: $\phi(t) = \Phi + \phi'(t)$ where Φ is the steady statistical average and $\phi'(t)$ is the fluctuating part. Concerning the phase-averaging, we follow the definition of Cantwell and Coles (1983) and we use the notation: $\phi(t) = \langle \Phi \rangle + \phi^*(t)$ where $\langle \Phi \rangle$ is the phase average and $\phi^*(t)$ corresponds to the turbulent fluctuation with respect to the phase-average.

3.1. Reynolds averaged quantities

Fig. 3 shows the Reynolds averaged velocity field within the 3-D measuring volume. The separation and reattachment due to the incidence are clearly illustrated. The wake structure displays two asymmetric recirculation regions.

Fig. 4 shows the statistical averaged streamlines and velocity component fields in the median plane. These fields show formation of two recirculation regions downstream of the trailing edge. The passage to zero of the streamwise velocity in the lower lobe occurs at $(x/c, y/c) = (-0.45, -0.1)$.

Fig. 4(b) shows the recirculation length obtained by the averaged streamwise velocity. The alternating vortices effect is shown in Fig. 4(c), by means of the averaged vertical velocity component.

Fig. 5 shows the *rms* values of the three velocity components. The streamwise *rms* velocity indicates a two-lobe structure with maximum values of order 0.32 (Fig. 5(a)). The v_{rms} component indicates an one-lobe structure with maximum values of order 0.42, near the position $(X/c; Y/c) = (0.44; -0.02)$. A strongly anisotropic behaviour of these *rms* components is therefore pointed out. This fact deserves to be taken into account whenever eddy-viscosity based turbulence behaviour laws are used for modelling this kind of highly inhomogeneous, anisotropic flows, governed by non-equilibrium turbulence effects. The Boussinesq approximation would lead for example to an isotropic behaviour of the turbulence stresses. Fig. 5(c) shows the averaged spanwise *rms* component, indicating a two-lobe structure with significant value areas located downstream of the separated shear layers.

Fig. 6 shows the three components of the Reynolds averaged shear stress tensor. The $\overline{u'v'}$ component is shown in Fig. 6(a). It displays a two-lobe structures with maximum values in the upper recirculation region. Fig. 6(b) underlines that maximum/minimum values of $\overline{u'w'}$ concentrate downstream, along the shear layers.

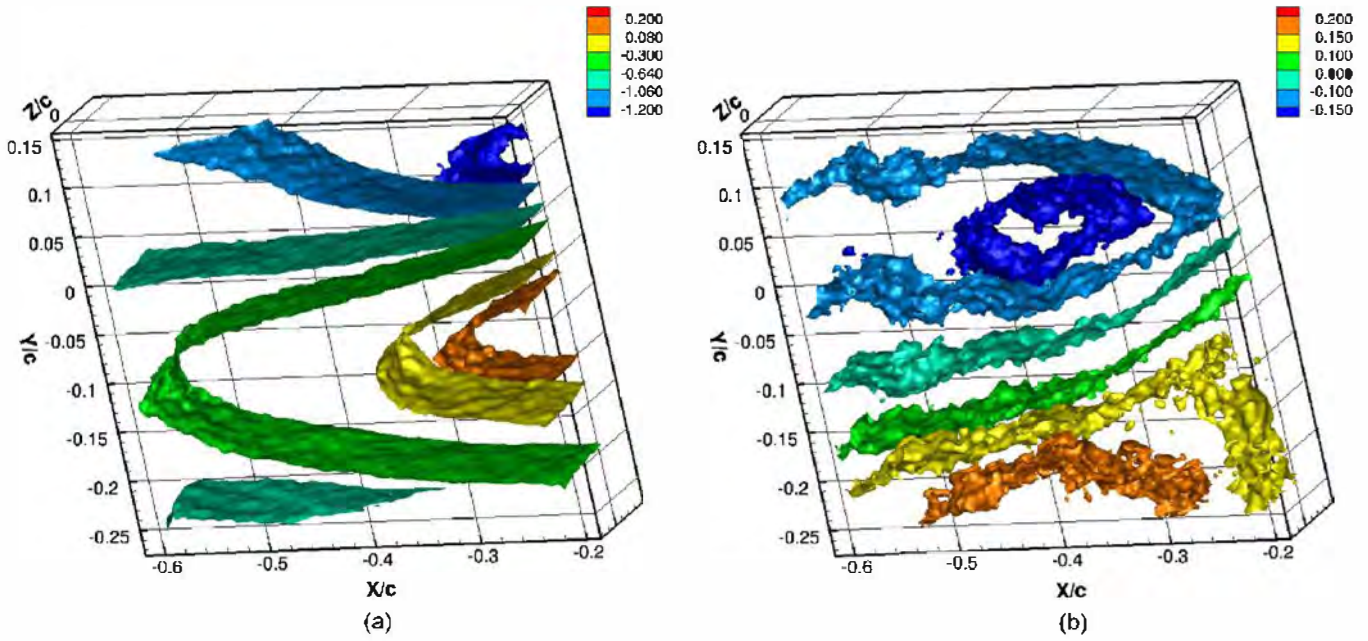


Fig. 3. Reynolds averaged quantities measured by Tomo-PIV: streamwise U velocity and vertical V velocity.

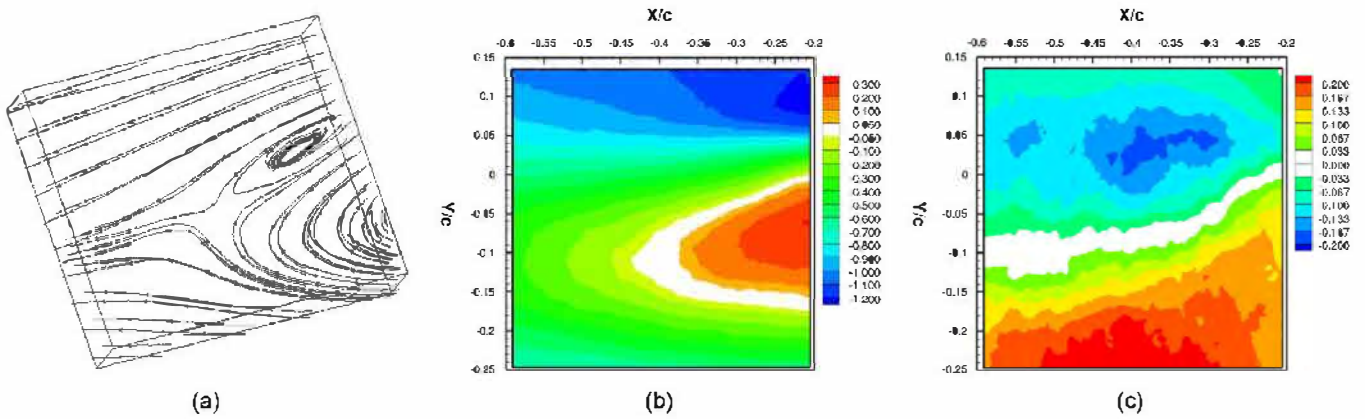


Fig. 4. Reynolds averaged quantities measured by Tomo-PIV: (a) streamlines in the whole volume (average streamlines), (b) streamwise (U) and (c) vertical velocities on the middle plane ($Z/c = 0$) (V).

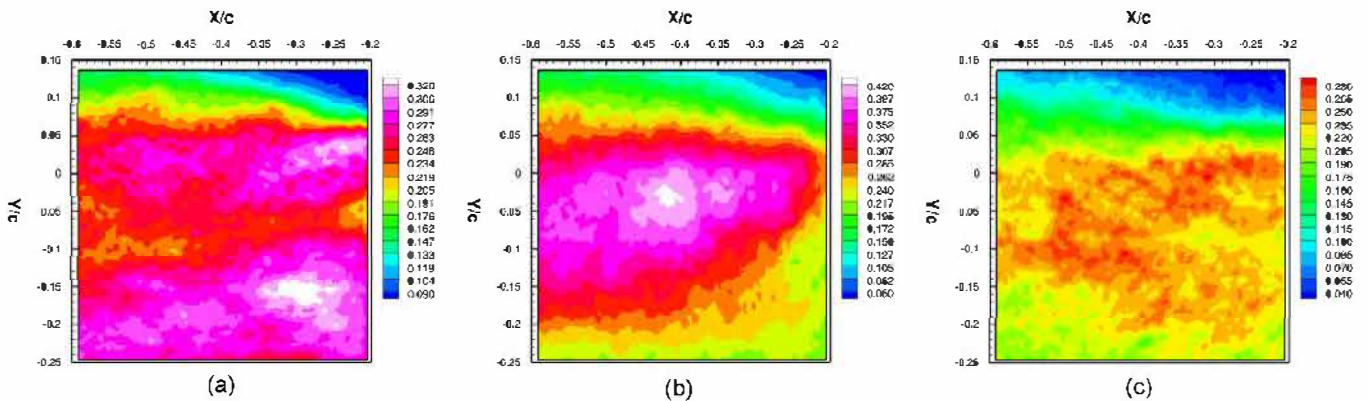


Fig. 5. rms values of the three velocity components in the middle plane. (a) u_{rms} , (b) v_{rms} and (c) w_{rms} .

3.2. Proper orthogonal decomposition and reconstruction

A 3-D Proper Orthogonal Decomposition (POD) analysis has been performed on the whole number of 3-D fields available from the Tomo-PIV measurements (Berkoov et al., 1993). The autocorrelation matrix is approximated by using the snapshots

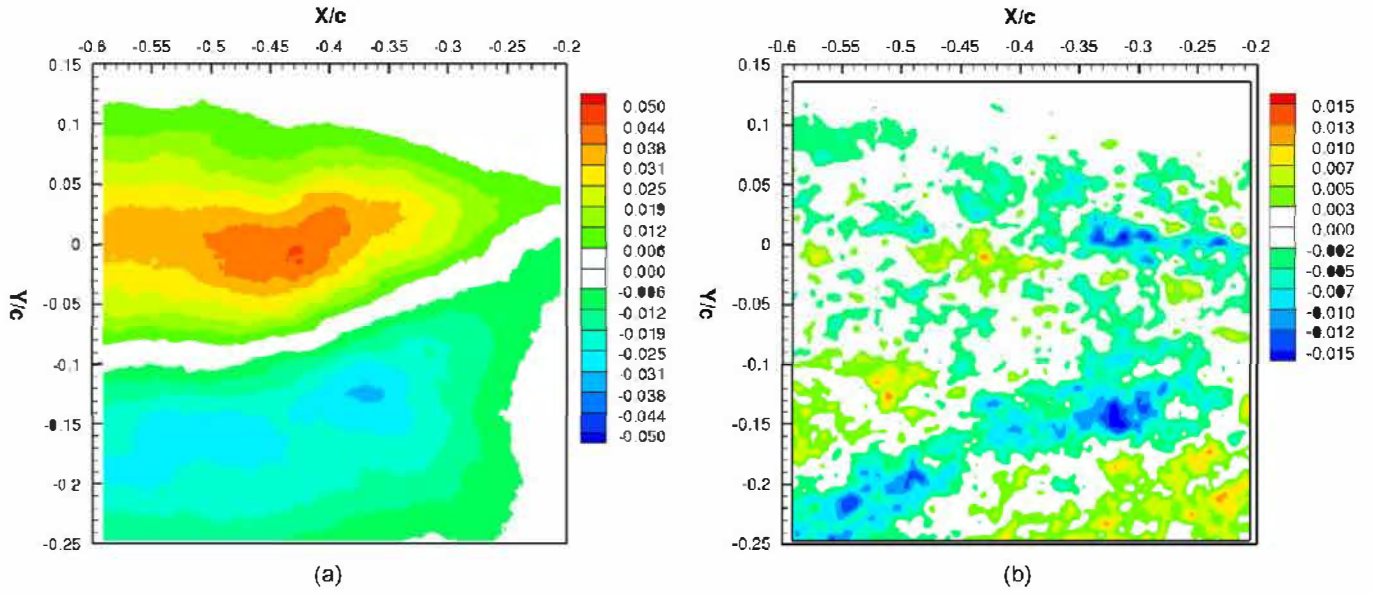


Fig. 6. Reynolds averaged shear stresses on the middle plane. (a) $\overline{u'v'}$ and (b) $\overline{u'w'}$.

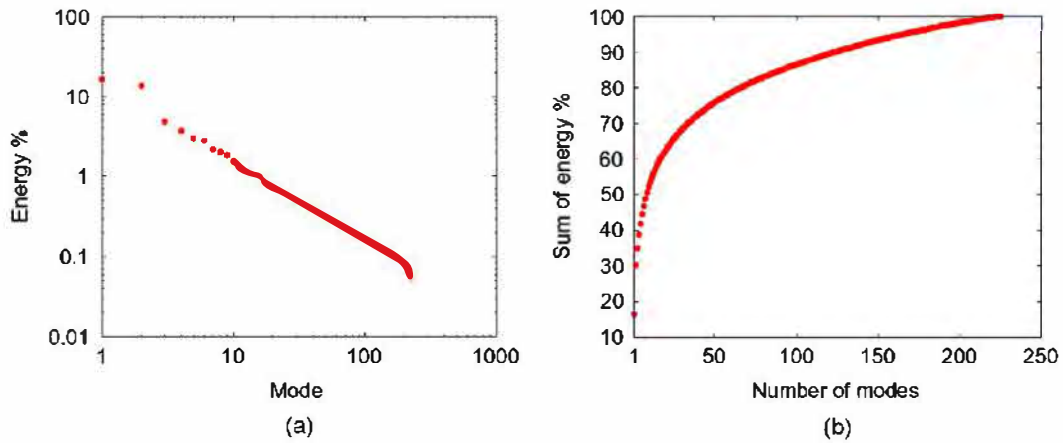


Fig. 7. POD decomposition: energy per mode and cumulative percentage of energy. (a) Energy per mode and (b) sum of energies.

method (Sirovich, 1987). The POD is used in the present study to find the most energetic flow structures by means of low order reconstruction and to determine the phase angle of each snapshot for phase-averaged quantities evaluation.

For a given flow, the velocity field $\mathbf{u}(X,Y,Z,t)$ is decomposed into a set of orthogonal basis functions $\psi(X,Y,Z)$, the modes, and a set of time-dependent coefficients $\zeta(t)$ as

$$\mathbf{u}(X,Y,Z,t) = \sum_{h=1}^N \zeta_h(t) \psi_h(X,Y,Z), \quad (2)$$

where N is the total number of available snapshots (here $N=225$). Low order reconstructions using a reduced order of modes are also possible. Prior to the POD decomposition, the statistical average has been removed from the snapshots fields, in order to provide a first POD mode directly linked to the vortex shedding.

Fig. 7(a) shows the evolution of the energy of each mode as a function of the mode's order. It is shown that the first six modes are characterised by a quite high energetic level. A slope change is shown between the sixth and seventh modes, indicating a change in the coherent structures' behaviour, that is more and more "contaminated" by the chaotic turbulence background in the higher order mode range. A similar change in the slope was shown in the POD analysis of snapshots issued from Three-Component Rapid PIV (3CTRPIV) by Perrin et al. (2007), in the wake of a circular cylinder at Reynolds number 140 000. This change may be associated to the non-linear interaction between the coherent vortices and the random turbulence due to smaller scale structures in the present high-Re strongly detached turbulent wake.

Fig. 7(b) shows the cumulative percentage of the energy as a function of modes. It is shown that an order of 60% of energy is contained in the first twenty modes. It is also obtained that the higher-order modes do not drastically lose their

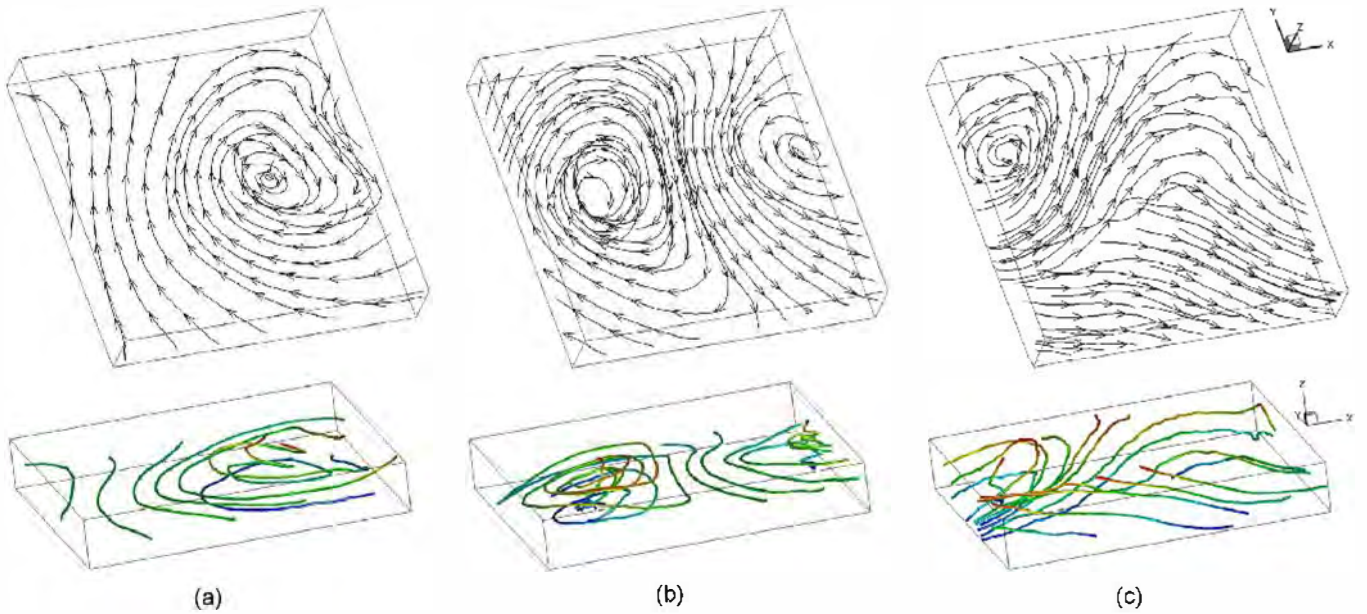


Fig. 8. First three POD modes. On bottom views, the streamlines are coloured according to the Z coordinate from blue to red in order to outline the 3-D effects. (a) First mode, (b) second mode and (c) third mode. (For interpretation of the references to color in this figure legend, the reader is referred to the web version of this article.)

energy as in lower Reynolds number flows, due to the significant effect of fine-scale turbulence intensity in the present flow. These aspects are to take into account in Reduced Order Modelling (ROM) development for high-Re detached flows, where a significant number of modes would be needed to capture turbulence effects, but a reduced number of modes (order of 20) would be needed to capture the most energetic vortex structures.

Fig. 8 shows the first three POD modes. The two first modes can be compared to the work by Perrin et al. (2009) concerning 3CTRPIV around a circular cylinder at high Reynolds number. Their shapes illustrate the alternating vortices effect that is obtained by reconstruction, as shown in the next paragraph. Although the first and second modes display a nearly symmetric shape in reference of the middle x -axis as in the case of the cylinder's wake, the third mode is strongly affected by the asymmetry in the wake pattern, due to the incidence. This mode is also the most affected by 3-D effects, along (X, Z) plans as shown in Fig. 8(c). Concerning the first and second modes, these 3-D effects are predominant in the central regions of the recirculations, Fig. 8(a) and (b).

Fig. 9 shows the POD reconstruction of an instantaneous flow field by a successively increasing number of modes. The 2-mode reconstruction clearly shows the alternating vortices effect and the formation of the saddle point (S) near the right-low part.

The six-mode reconstruction shows three-dimensionality formation near the saddle point (streamlines crossing in Fig. 9(b) is due to 3-D prospective effects). The 3-D effect in the center of the recirculation region becomes more predominant with the 9-mode reconstruction. The center of the upper recirculation and the saddle point three-dimensionality appear more clearly with the 25-mode reconstruction, compared to the instantaneous field. The overall reconstruction shows that the most energetic coherent vortex pattern can be achieved by using a moderate number of POD modes. Three-dimensional effects of the coherent vortices can appear with the use of a moderate number of modes for the POD reconstruction, despite the high-Reynolds flow. This is an important fact concerning further developments using Reduced Order Modelling, as for example by Bourguet et al. (2009), or by Noack et al. (2003). However, the present study indicates that smaller-scale turbulence effects, mostly affected by three-dimensionality, need a higher number of POD modes.

Fig. 10 shows the 2-mode POD reconstruction of the modulus (norme) of the vorticity vector field, superimposed with the streamlines reconstruction and compared with the instantaneous vorticity field, that displays a high turbulence level leading to maximum fluctuating vorticity values of order 100. The two-mode POD reconstruction makes appearance of the coherent vorticity pattern due to the alternating von Kármán eddies. Their maximum dimensionless vorticity amount is found to be of order 20 and located in the center of the main recirculation area. The difference in the vorticity values is due to the small scale turbulence filtering operated by the 2-mode POD reconstruction. The lower vortex region is less clearly illustrated because of the dimensions of the domain.

3.3. Phase averaging

Phase identification using POD for a wake past a plate was first proposed by Ben Chiekh et al. (2004) for an angle of attack of 90° . Following this study van Oudheusden et al. (2005) applied the method to the square cylinder, and Perrin et al. (2008) to the circular cylinder at high Reynolds number. The present study uses the same method to perform phase identification. The phase

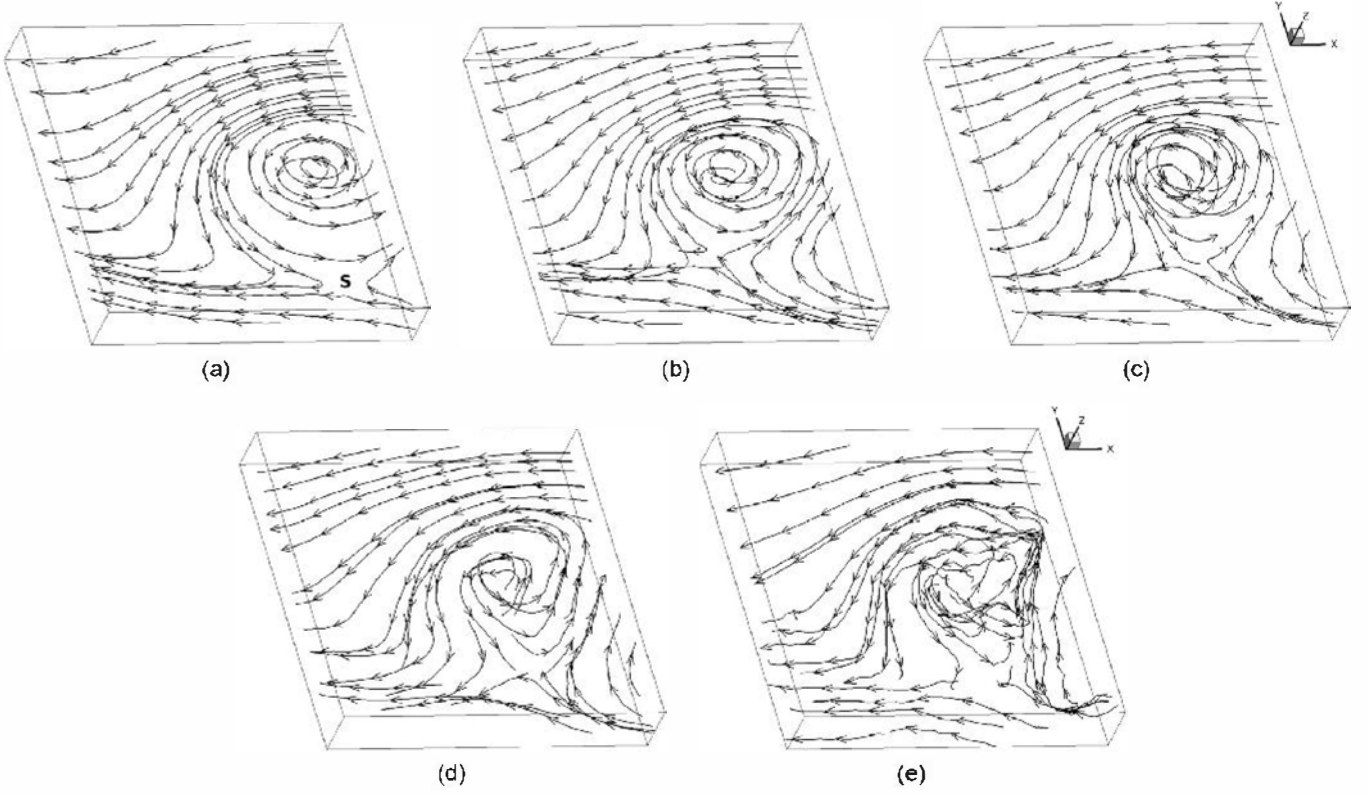


Fig. 9. Low order POD reconstruction of an instantaneous streamlines field. (a) 2-mode reconstruction, (b) 6-mode reconstruction, (c) 9-mode reconstruction, (d) 25-mode reconstruction and (e) instantaneous field.

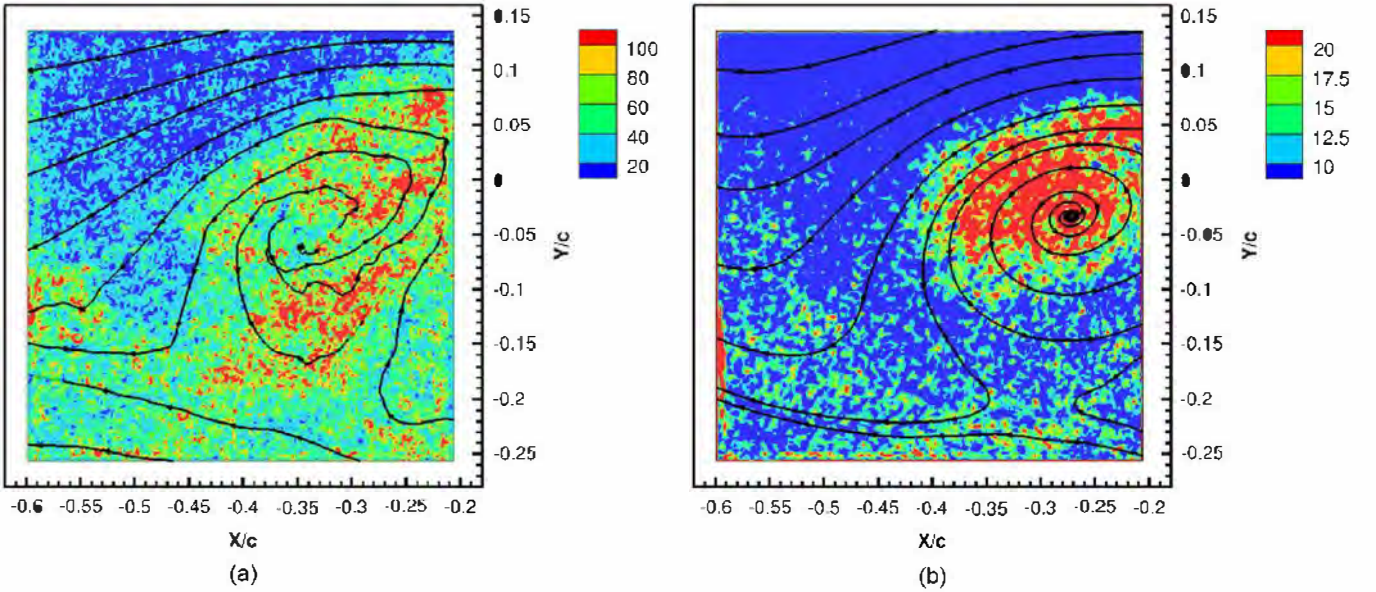


Fig. 10. Instantaneous Ω vorticity vector norm on the middle plane (a) and 2-mode POD reconstruction of the vorticity norm (b) referring to the flow snapshot of Fig. 9.

angle $\beta(t)$ is defined for each vector field of a physical quantity $\mathbf{u}(x,y,z,t)$ as

$$\beta(t) = \arctan\left(\frac{\zeta_2(t)\sqrt{\lambda_1}}{\zeta_1(t)\sqrt{\lambda_2}}\right), \quad (3)$$

where λ_1 and λ_2 are the two first eigenvalues obtained from POD. Fig. 11 shows the number of snapshots obtained per phase angle, according to the above algorithm.

Eight phases are shown, as in Lam (1996), corresponding to equidistant phase intervals in a whole vortex shedding's cycle. The number of averaged snapshots per phase is shown in Fig. 11.

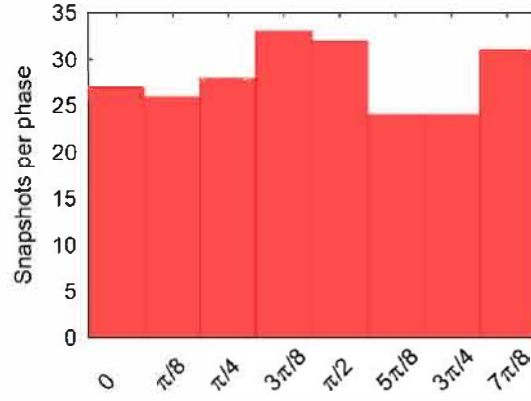


Fig. 11. Snapshots per phase following phase identification.

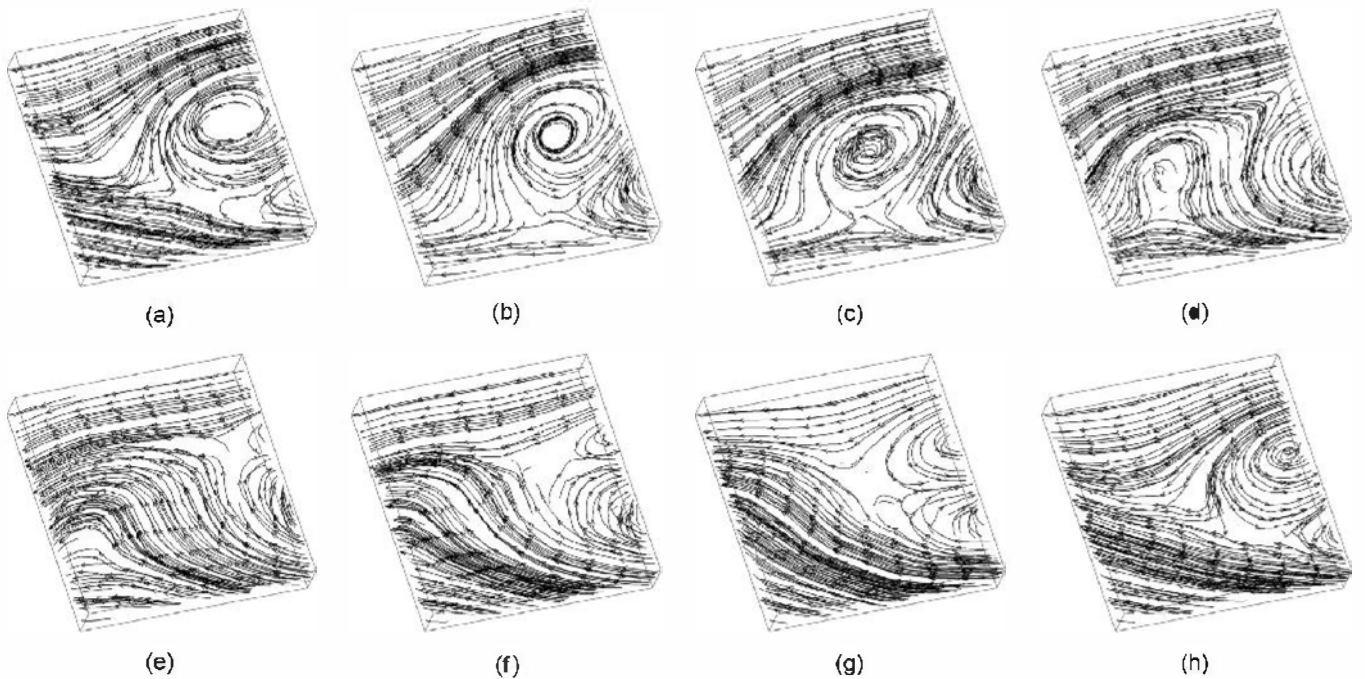


Fig. 12. Phase averaged streamlines. (a) $\beta = 0$, (b) $\beta = \frac{\pi}{8}$, (c) $\beta = \frac{\pi}{4}$, (d) $\beta = \frac{3\pi}{8}$, (e) $\beta = \frac{\pi}{2}$, (f) $\beta = \frac{5\pi}{8}$, (g) $\beta = \frac{3\pi}{4}$ and (h) $\beta = \frac{7\pi}{8}$.

Fig. 12 shows the vortex shedding motion according to the eight phase instants, where the first and last illustrate practically a quasi-periodic phenomenon. The formation of the saddle point S between the vortices and the convective region are illustrated within this cycle, as well as the 3-D shape of the main recirculation region. Furthermore, the formation of the lower, weaker detached vortex is also shown within this period. Both, the thin shear layers above and below the alternating vortices are also clearly formed. The detection of these thin shear layer interfaces between rotational and irrotational regions is of importance for aeroacoustics studies, as well as for assessment of the predictive abilities of CFD methodologies, that usually have the tendency of producing excessively diffusive interfaces and therefore, drag overprediction. These aspects, together with adequate treatment of turbulent interfaces by upscale turbulence modelling approaches are discussed in [Deri et al. \(2011\)](#), [Ouvrard et al. \(2010\)](#) and in [Eames et al. \(2011\)](#).

Fig. 13 shows the phase-averaged iso- U velocity component in the same period. The dynamics of the main recirculation region are clearly shown. The maximum absolute value of the U velocity appears in the upper shear layer and is of order 1.20. The formation and convection of the central area of the recirculation region (white area) within the cycle of the main vortex shedding are provided. These variations are in accordance with the streamlines dynamics presented in [Fig. 12](#).

4. Conclusions

The present study is a first application of the Tomo-PIV technique at high Reynolds number ($Re=200\,000$) in the turbulent flow past a thin flat plate. The experiments have been carried out in the $S4$ wind tunnel of IMFT. The high Reynolds number and the gas flow represented difficult aspects to overcome in order to achieve the present Tomo-PIV. These measurements are to our knowledge original results in the state of the art. The present study provides the separated

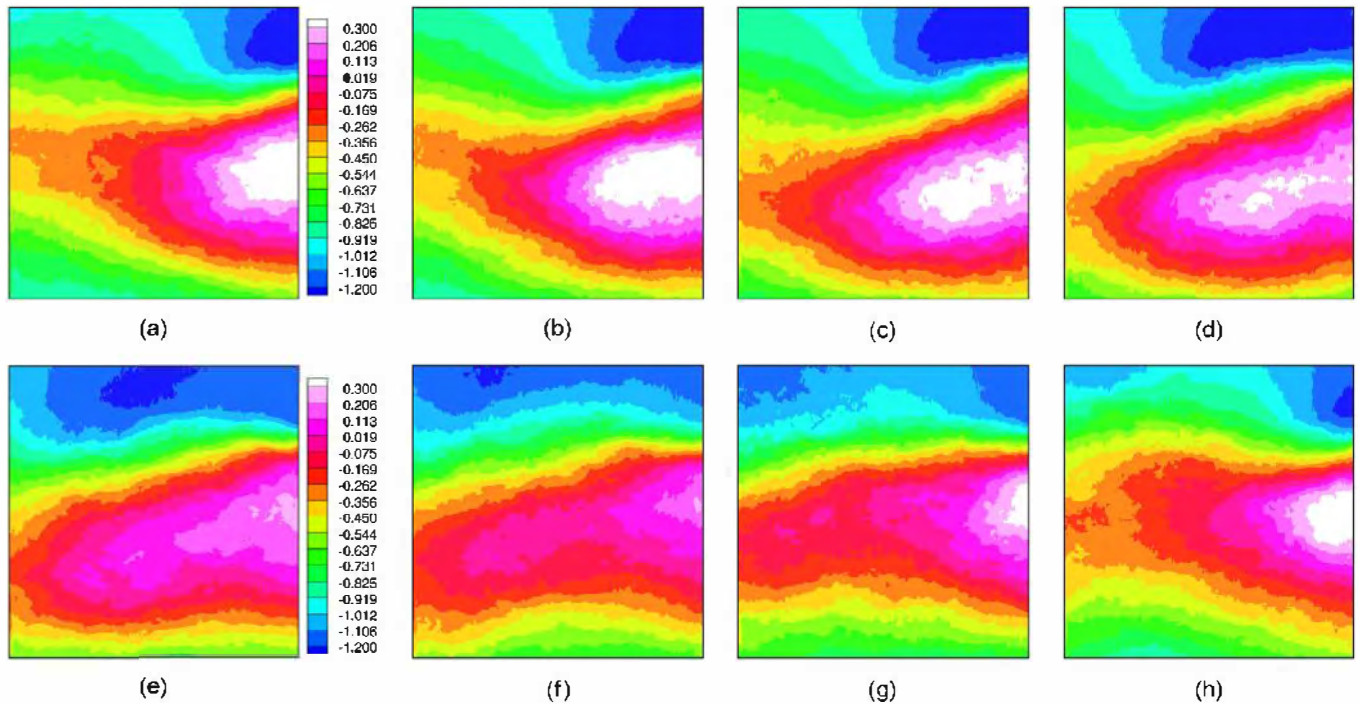


Fig. 13. Phase averaged streamwise velocity $\langle U \rangle$ on the middle plane of the measured volume (i.e. $Z=0$). (a) $\beta = 0$, (b) $\beta = \frac{\pi}{8}$, (c) $\beta = \frac{\pi}{4}$, (d) $\beta = \frac{3}{8}\pi$, (e) $\beta = \frac{\pi}{2}$, (f) $\beta = \frac{5}{8}\pi$, (g) $\beta = \frac{3}{4}\pi$ and (h) $\beta = \frac{7}{8}\pi$.

flow structure and the coherent vortex pattern, the recirculation region topology and the turbulent stresses fields, by means of statistical averaging. The study of the turbulent stresses has quantified a strongly anisotropic character of the turbulence structure in the near wake.

Furthermore, the present study provides the dynamics of the coherent vortex structures in the near wake by means of POD decomposition and reconstruction. A strong three-dimensional effect is detected even for the first POD modes. The influence of turbulence on the number of modes needed to represent the coherent vortex patterns is analysed. The alternating eddies pattern can be captured by means of 6 modes reconstruction. Higher-order modes contribute to three-dimensional spanwise modulation of the coherent pattern and to the appearance of smaller-scale fluctuations. Phase-averaged analysis performed by classification of the tomo-PIV snapshots according to the two first POD modes allowed extraction of the vortex shedding dynamics among the overall turbulent background.

The present study allows for a direct comparison of the *three-dimensional* POD modes with the modes obtained by 3-D numerical simulation of the present flow thanks to the Tomographic-PIV. These aspects can be useful for further developments and validation of turbulence modeling studies for unsteady, strongly detached turbulent flows at high Reynolds number.

Acknowledgements

The present study has been sponsored by the Foundation STAE-RTRA-research program EMMAV. The authors are grateful to the STAE-RTRA Foundation for having funded this study and especially the post-doc of Dr. E. Deri. The LaVision Company contribution is highly acknowledged by IMFT for the time devoted in this study and for the two high-resolution cameras put at the disposal of the present experiments. The authors thank R. Soeparno, C. Korbuly, the Technical Service directed by J.M. Sfedj at IMFT, the Service of Signal and Image Processing directed by J.F. Alquier and the Computing service directed by C. Nicolas, for their technical contribution to the experimental set-up and for the computing facility arrangements to treat a considerable size of data. They thank F. Grossi for his valuable contribution in the final editing, as well as T. de Faramond for language improvements.

References

- Abernathy, F.H., 1962. Flow over an inclined plate. *Journal of Basic Engineering* 84, 380–388.
- Beckwith, R.M.H., Babinsky, H., 2009. Impulsively started flat plate flow. *Journal of Aircraft* 46 (6), 2186–2188.
- Ben Chiekh, M., Michard, M., Grosjean, N., Béra, J.-C., 2004. Reconstruction temporelle d'un champ aérodynamique instationnaire à partir de mesures PIV non résolues dans le temps. In: 9ème Congrès de Vélométrie Laser. Bruxelles, Belgium.
- Berkooz, G., Holmes, P., Lumley, J.L., 1993. The proper orthogonal decomposition in the analysis of turbulent flows. *Annual Review of Fluid Mechanics* 25, 539–575.
- Bourguet, R., Braza, M., Sevrain, A., Bouhadjji, A., 2009. Capturing transition features around a wing by reduced-order modeling based on compressible Navier–Stokes equations. *Physics of Fluids* 21, 094104.

- Breuer, M., Jovičić, N., Mazev, K., 2003. Comparison of DES, RANS and LES for the separated flow around a flat plate at high incidence. *International Journal for Numerical Methods in Fluids* 41, 357–388.
- Cantwell, B., Coles, D., 1983. An experimental study of entrainment and transport in the turbulent near wake of a circular cylinder. *Journal of Fluid Mechanics* 136, 321–374.
- Chassaing, P., George, J., Claria, A., Sananes, F., 1974. Physical characteristics of subsonic jets in a cross-stream. *Journal of Fluid Mechanics* 62 (1), 41–64.
- Deri, E., Ouvrard, H., Braza, M., Hunt, J.C.R., Cazin, S., Cid, E., Hoarau, Y., Harran, G., 2011. Capturing turbulent interfaces in wake flows by means of the OES approach. *Journal of Physics, Conference Series* 318, 092002.
- Eames, I., Hunt, J.C.R., Braza, M., da Silva, C., Westerweel, J., 2011. Interfaces in turbulence and implications for advanced modeling methods. *ERCOFTAC Bulletin* 88, 18–22.
- Elsinga, G., Scarano, F., Wieneke, B., van Oudheusden, B.W., 2006. Tomographic particle image velocimetry. *Experiments in Fluids* 41, 933–947.
- Fage, A., Johansen, F.C., 1927. On the flow of air behind an inclined flat plate of infinite span. *Proceedings of the Royal Society of London. Series A* 116 (773), 170–197.
- Gahemi, S., Scarano, F., 2010. Multi-pass light amplification for tomographic particle image velocimetry applications. *Measurement Science and Technology* 21, 127002.
- Hsu, C.C., Huang, C.I., 2008. Vortex simulations of the flow-field of a flat plate with a non zero angle of attack. *Journal of Mechanics* 24 (3), N35–N38.
- Lam, K.M., 1996. Phase-locked eduction of vortex shedding in flow past an inclined flat plate. *Physics of Fluids* 8 (5), 1159–1168.
- Lam, K.M., Leung, M.Y.H., 2005. Asymmetric vortex shedding flow past an inclined flat plate at high incidence. *European Journal of Mechanics B/Fluids* 24, 33–48.
- Lam, K.M., Wei, C.T., 2010. Numerical simulation of the vortex shedding from an inclined flat plate. *Engineering Applications of Computational Fluid Mechanics* 4 (4), 569–579.
- Leder, A., 1991. Dynamics of fluid mixing in separated flows. *Physics of Fluids A* 3 (7), 1741–1748.
- Lee, J.S., Lee, S.H., 2012. Fluid–structure interaction analysis on a flexible plate normal to a free stream at low Reynolds numbers. *Journal of Fluids and Structures* 29, 18–34.
- Noack, B.R., Afanasiev, K., Morzynski, M., Tadmor, G., Thiele, F., 2003. A hierarchy of low-dimensional models for the transient and post-transient cylinder wake. *Journal of Fluid Mechanics* 497, 335–363.
- Ouvrard, H., Braza, M., Hunt, J.C.R., Barbut, G., Hoarau, Y., 28–30 June 2010. Capturing turbulent interfaces in wake flows by means of the OES approach. In: *EUROMECH Colloquium 517: Interfaces and Inhomogeneous Turbulence*. UCL London, invited presentation.
- Pelletier, A., Mueller, T.J., 2000. Low Reynolds number aerodynamics of low-aspect-ratio, thin/flat/cambered-plate wings. *Journal of Aircraft* 37 (5), 825–832.
- Perrin, R., Braza, M., Cid, E., Cazin, S., Barthet, A., Sevrain, A., Mockett, C., Thiele, F., 2007. Obtaining phase averaged turbulence properties in the near wake of a circular cylinder at high Reynolds number using POD. *Experiments in Fluids* 43, 341–355.
- Perrin, R., Braza, M., Cid, E., Cazin, S., Chassaing, P., Mockett, C., Reimann, T., Thiele, F., 2008. Coherent and turbulent process analysis in the flow past a circular cylinder at high Reynolds number. *Journal of Fluids and Structures* 24, 1313–1325.
- Perrin, R., Braza, M., Cid, E., Cazin, S., Sevrain, A., Harran, G., 2009. The IMFT circular cylinder experiment. In: *DESider—A European Effort on Hybrid RANS-LES Modelling*. Springer, pp. 90–103.
- Perry, A.E., Steiner, T.R., 1987. Large-scale vortex structures in turbulent wakes behind bluff bodies. part 1. vortex formation processes. *Journal of Fluid Mechanics* 174, 233–270.
- Rebuffet, P., 1950. *Aérodynamique expérimentale*. Dunod.
- Shi, L.L., Liu, Y.Z., Yu, J., 2010. PIV measurement of separated flow over a blunt plate with different chord-to-thickness ratios. *Journal of Fluids and Structures* 26, 644–657.
- Sirovich, L., 1987. Turbulence and the dynamics of coherent structures part III: dynamics and scaling. *Quarterly of Applied Mathematics* 45 (3), 583–590.
- Steiner, T.R., Perry, A.E., 1987. Large-scale vortex structures in turbulent wakes behind bluff bodies. Part 2. Far-wake structures. *Journal of Fluid Mechanics* 174, 271–298.
- van Oudheusden, B.W., Scarano, F., van Hinsberg, N.P., Watt, D.W., 2005. Phase-resolved characterization of vortex shedding in the near wake of a square-section cylinder at incidence. *Experiments in Fluids* 39, 86–98.
- Westerweel, J., Scarano, F., 2005. Universal outlier detection for PIV data. *Experiments in Fluids* 39, 1096–1100.
- Wick, B.H., 1954. Study of the Subsonic Forces and Moments on an Inclined Plate of Infinite Span. Technical Report. TN 3221, National Advisory Committee for Aeronautics, Washington, USA.